Published in IET Generation, Transmission & Distribution
Received on 28th August 2013
Revised on 28th November 2013
Accepted on 31st December 2013
doi: 10.1049/iet-gtd.2013.0616

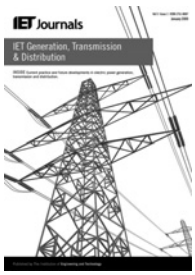

ISSN 1751-8687

Real-time transient stability assessment based on centre-of-inertia estimation from phasor measurement unit records

Jaime C. Cepeda[1], José L. Rueda[2], Delia G. Colomé[3], Diego E. Echeverría[1]

[1]Research and Development Department, Centro Nacional de Control de Energía (CENACE), Av. Atacazo y Panamericana Sur km 0, 171112 Quito, Ecuador
[2]Institute of Electrical Power Systems (EAN), University Duisburg-Essen, Bismarckstrasse 81, 47057 Duisburg, Germany
[3]Instituto de Energía Eléctrica (IEE), Universidad Nacional de San Juan, Avenida Libertador 1109 (O), 5400 San Juan, Argentina
E-mail: jcepeda@cenace.org.ec

Abstract: Several smart grid applications have recently been devised in order to timely perform supervisory functions along with self-healing and adaptive countermeasures based on system-wide analysis, with the ultimate goal of reducing the risks associated with potentially insecure operating conditions. Real-time transient stability assessment (TSA) belongs to this type of applications, which allows deciding and coordinating pertinent corrective control actions depending on the evolution of post-fault rotor-angle deviations. This study presents a novel approach for carrying out real-time TSA based on prediction of area-based centre-of-inertia (COI) referred rotor angles from phasor measurement unit (PMU) measurements. Monte Carlo-based procedures are performed to iteratively evaluate the system transient stability response, considering the operational statistics related to loading condition changes and fault occurrence rates, in order to build a knowledge database for PMU and COI-referred rotor-angles as well as to screen those relevant PMU signals that allows ensuring high observability of slow and fast dynamic phenomena. The database is employed for structuring and training an intelligent COI-referred rotor-angle regressor based on support vector machines [support vector regressor (SVR)] to be used for real-time TSA from selected PMUs. Besides, the SVR is optimally tuned by using the swarm variant of the mean-variance mapping optimisation. The proposal is tested on the IEEE New England 39-bus system. Results demonstrate the feasibility of the methodology in estimating the COI-referred rotor angles, which enables alerting about real-time transient stability threats per system areas, for which a transient stability index is also computed.

1 Introduction

In recent years, a number of factors such as transitioning energy policies, market pressures, slow transmission expansion, bulk power transfers over long distances and increasing environmental constraints, have pushed power systems to be frequently operated close to their technical limits [1]. Under these conditions, some critical contingencies may lead to major consequences, including widespread disruptions or even blackouts, whose root causes are occasionally attributed to large rotor-angle deviations [2]. Thus, real-time assessment of large-disturbance rotor-angle stability (i.e. transient stability—TS), which is concerned with the ability of a power system to maintain synchronism after being subjected to a large disturbance, is receiving a renewed interest from power system community [3].

Traditionally, transient stability assessment (TSA) has been conducted by using offline dynamic simulations for a given set of credible contingencies. This framework has been widely used for the designing and tuning of protective and control systems and to provide guidelines for secure operations as well. By contrast, real-time TSA is appropriate for evaluating the progress of actual transient phenomena occurring in a power system [4]. In view of this, several smart grid applications have been developed to improve monitoring, protection and control tasks in real time, which are mainly based on emerging technologies such as phasor measurement units (PMUs) and wide-area monitoring, protection and control systems [5–7]. The use of PMUs facilitates the measurement of electrical quantities at high sampling rates, hence it allows tracking post-fault transient evolution in real time [5]. In this connection, several research works have been carried out in order to predict and assess possible transient instability in real time from PMU measurements [4–26]. Moreover, post-contingency corrective control actions could be also executed within real time as long as reliable TSA is previously guaranteed [5].

For instance, the so-called piecewise constant-current load equivalent (PCCLE) approach is presented in [8] whose aim is to perform on-line TSA. In [9], the research work introduced in [8] has been extended for proposing two

additional techniques: (i) piecewise constant transfer admittance equivalent (PCTAE); and (ii) implicitly decoupled PQ integration (IDPQI), in addition to PCCLE. Although the methods PCCLE and PCTAE allow knocking out the algebraic equations throughout the approximations of the power flow solution by pieces, IDPQI reduces the integration time of the set of differential/algebraic equations that describe the post-fault power system.

A method based on fuzzy hyper-rectangular composite neural network is proposed in [10] for the prediction of oscillations during TS phenomenon using a short-term time window of post-contingency phasor measurements.

An autoregressive model for the prediction of power system loss of synchronism is depicted in [11]. Two types of temporal series data are employed in order to identify the model, that is: (i) the voltage phasor angle difference between two substations; and (ii) the rotor angles of generators. On the other hand, a measure of the angular stability margin, called branch impedance trajectory sensitivity, is proposed in [12].

An algorithm for on-line prediction of TS, based on PMU measurements together with models from energy management system (EMS) functions, is proposed in [13]. From EMS pre-fault models and the post-fault system topology, a reduced model of the post-contingency power system is built. This reduced model only keeps the generator terminal buses, and the method assumes that PMUs are already located at each of these buses. The TS prediction is carried out via time domain simulations of the reduced network together with an algorithm that permits estimating the rotor angles of power plants. The required time domain simulations restrict the feasibility for real-time applications of this method.

A method for predicting the TS based on wide area measurement system (WAMS) data is presented in [14]. This approach uses PMU measurement, identification of coherent groups of generators, system equivalent reduction, and stability prediction algorithms in order to accomplish its aim. Once the perturbation occurs, the original system is reduced via clustering techniques applied to the dynamic response. Then, the future angle trajectories and the angular frequency of generators are predicted via time domain simulations. This task hinders the real-time application of this method. In addition, the methodology applies the classic generator model, which constitutes an unnecessary limitation of the algorithm.

Some methods for real-time TSA were introduced in [15], from which emergency single machine equivalent (E-SIME) seems attractive for real-time applications. Basically, this method uses multi-machine rotor angles (δ_i) and the system accelerating power (Pa) for synthesising the so-called one machine infinite bus (OMIB) equivalent, which eases the prediction of transient instability from PMU data [15–17]. Nevertheless, in this approach, the derivation of mechanical variables together with the prediction of the Pa—δ curves entail relatively significant time delays and numerical inaccuracies. Also, a scheme based on visualisation of phase-space curves of critical variables, which allows identifying patterns that could alert about a possible collapse (i.e. early warning) was reported in [18]. However, the fast automatic update of the curves to continuously unveil their similarities is still to be overcome. A technique for classifying the TS status of a power system following a large disturbance, based on synchronously measured samples of voltage phasor magnitudes at major generation centres, is proposed in [19]. The samples, acquired immediately after fault clearance, constitute the inputs of a binary classifier based on support vector machines (SVM), used to identify the actual TS status. This approach assumes that PMUs are available at all generators' terminal buses, without performing feature extraction to reduce the dimensionality of the input data of the classifier, which indeed adversely affects the SVM training stage. On the other hand, an approach for predicting the TS status in real time, based on data mining techniques and SVM, is presented in [5]. This method considers PMUs properly located at specific buses (which is more realistic due to limited availability of resources for real-time data handling) and uses time series data mining to reduce the classifier's input features. Remarkably, the last two methods provide a binary indication of the actual stability status (i.e. whether the system is stable or not) without quantifying the actual TS level, a measure that allows ascertaining the distance to the TS security border.

A vulnerability assessment (VA) method for quickly assessing the multi-area power system post-contingency vulnerability status, mainly regarding to rotor-angle stability, is developed in [20]. This method uses PMU data to compute wide-area severity indices (WASI), as an extension of the severity indices firstly presented in [21]. These WASI are calculated in the frequency domain through applying the short-time-Fourier-transform to data obtained from PMUs located in specific system buses, determined by a coherency criterion defined in [22] and improved in [23]. A systematic scheme for rapidly classifying the stability status resulted from WASI using fuzzy rule-based classifiers is presented [24]. This classifier uses large-size decision trees (DTs) to generate initial accurate classification boundaries for decision making as early as 1 or 2 s after fault clearing. A WASI-based model-predictive framework for determining fast catastrophe precursors in a bulk power system has been stated in [25]. These fast catastrophe predictors use random-forest (RF) learning in order to increase the classification accuracy, showing excellent performance as regards typical DTs. In [26], a comparison between several data mining classifiers, such as artificial neural networks, SVM, DT, Fuzzy DT, Fuzzy ID3 (Iterative Dichotomiser 3), and RF is performed; from which, RF-based predictor is the only one to achieve more than 99.0% of accuracy based on WASI. However, RF presents poorly transparent characteristics and might present over-fitting problems. In this connection, a more transparent predictor is suggested to be used in [26] at the expense of loss of accuracy. WASI offer a novel concept in power system real-time VA that reasonably permits estimating the tendency of the system to change its conditions to a critical state. Nevertheless, these indices present the problem of showing a considerable large overlapping zone. For instance, test results in [25] conclude that '75% of stable cases verify the relationship FastWASI300 ms <-2.5, while for 75% unstable cases, FastWASI300 ms >-2.5'. This fact denotes that the overlapping zone is formed by 25% of stable cases belonging to the region of the unstable cases and vice versa. This large overlapping range is one of the reasons of classification difficulties, and this issue has been surpassed via a most sophisticated classifier (RF-based predictor).

In summary, although the mentioned proposals have given a new challenging viewpoint regarding real-time TSA, some drawbacks have to be still tackled, such as: to obtain better accuracy in the results; and to contemplate rational PMU locations instead of considering PMUs at every generation buses. Then, more appropriate mathematical tools should be developed in order to better adapt to the power system

doi: 10.1049/iet-gtd.2013.0616

dynamic variables, considering a more realistic PMU availability.

Thus, in this paper, a novel approach, aimed at providing a quick quantification of the actual TS level, via the computation of a TS index (TSI), is introduced. It employs a SVM regressor (i.e. support vector regressor (SVR)) to predict area-based COI-referred rotor angles from selected PMU measurements. The input dimensionality reduction and training tasks are performed through mining data obtained via Monte Carlo (MC)-based procedures, whereas the tuning of the SVR is done by using the swarm variant of the mean-variance mapping optimisation. The main advantage of this method is that it considers PMU rational locations while providing good accuracy results. The paper is organised as follows: Section 2 briefly reviews the theoretical background on COI-referred rotor angles and associated PMU electric areas. Section 3 gives an overview of the proposed approach for real-time COI-referred rotor-angle estimation and TSI computation. Simulation tests and discussion on the performance of the proposal are provided in Section 4 and Section 5. Finally, Section 6 summarises the concluding remarks.

2 Theoretical background

2.1 COI-referred rotor angles

Mathematically, for each synchronous generator in a power system, the behaviour of rotor-angle δ_i ($i = 1, 2, \ldots n$) is determined by the swing equation [27]

$$\frac{\mathrm{d}\delta_i(t)}{\mathrm{d}t} = \omega_i(t) - \omega_o \tag{1}$$

$$\frac{\mathrm{d}\omega_i(t)}{\mathrm{d}t} = \frac{1}{M_i}\left[\mathrm{Pm}_i(t) - \mathrm{Pe}_i(t)\right] \tag{2}$$

where M_i, Pm_i, Pe_i and ω_i stand for inertia moment, mechanical power input, electrical power output and rotor speed of the ith generator, respectively.

The solution of these differential equations represents the time domain dynamic system trajectory, which allows determining the dynamic response of all the state variables (i.e. δ_i and ω_i). The computed rotor angles can then be used for determining the COI-referred rotor angles [28], and subsequently a TSI, which represents the stability of each area of a power system (i.e. area-based COI-referred rotor-angle index), can be calculated. This TSI is based on an equivalent inertia representing the total inertia of the generators located in each area.

Considering that all generators in an area are coherent following a perturbation, an equivalent single large machine representing all generators in that area can be assumed without excessive errors. In this connection, [28] defines the area equivalent rotor-angle concept, which represents the average rotor-angle of the N_j generators belonging to area j. Nevertheless, since each area can comprise machines of different size, an arithmetic average does not properly represent the inertial influence of each generator, because it does not accomplish the COI definition. Thus, this paper considers an inertial area equivalent rotor angle, defined by (3) and (4), which could be viewed as the angle of the equivalent inertial centre of each electric area

$$\delta_{\mathrm{COI}_j} = \frac{1}{M_j}\sum_{i=1}^{N_j} M_i\delta_i \tag{3}$$

$$M_j = \sum_{i=1}^{N} M_i \tag{4}$$

where $\delta_{\mathrm{COI}\,j}$ and M_j are the inertial area equivalent rotor angle, and the total inertia moment of the jth area, whereas M_i and δ_i denote inertia moment and rotor-angle of ith machine belonging to jth area, respectively.

Considering a total number of r areas in a power system, the COI of the system can be defined as follows

$$\delta_{\mathrm{COI}_{\mathrm{System}}} = \frac{1}{M_T}\sum_{j=1}^{r} M_j\delta_{\mathrm{COI}_j} \tag{5}$$

$$M_T = \sum_{j=1}^{r} M_j \tag{6}$$

where $\delta_{\mathrm{COI\ System}}$ is the system COI equivalent rotor angle, and M_T is the total inertia moment of the system.

Then, the COI-referred rotor-angle of the jth area $\left(\delta_j^{\mathrm{COI}_{\mathrm{System}}}\right)$ is defined as follows

$$\delta_j^{\mathrm{COI}_{\mathrm{System}}} = \delta_{\mathrm{COI}_j} - \delta_{\mathrm{COI}_{\mathrm{System}}} \tag{7}$$

The TSA criterion, founded on area-based COI-referred rotor angles, establishes that, if the COI-referred rotor-angle of any area $\left(\delta_j^{\mathrm{COI}_{\mathrm{System}}}\right)$ goes out of step after a fault is cleared (i.e. surpass 180°), then the area is said to be unstable, whereas, if it remains in equilibrium, then the area is said to be stable [28].

It is worth mentioning that the values that $\delta_j^{\mathrm{COI}_{\mathrm{System}}}$ might reach depend on the system dynamic configuration, the contingency magnitude and location, the fault clearing time and the power system controllers installed in the system. Historically, the role of excitation systems to improve the stability of power systems has steadily increased. Modern excitation systems are capable of providing a virtually immediate response with high threshold voltages. The combination of high stress capacity of the field windings and the use of auxiliary signs of stabilisation, substantially contributes to the improvement of the overall dynamic response of the systems. In this connection, the automatic voltage regulators contribute to improve the TS of the power system, and then, to reduce the maximum values of $\delta_j^{\mathrm{COI}_{\mathrm{System}}}$ and to improve the TS margins or indices.

2.2 Probabilistic-based PMU monitoring locations and associated PMU coherent areas

Several real-time TSA methods assume that PMUs are located at every bus of the power system. Although it is a valid assumption, it is not, however, entirely practical, since extremely sophisticated communication networks would be required. Additionally, considering this ideal situation, the huge volumes of real-time data would be infeasible to be analysed within short time frames. Thus, a strategic selection of PMUs monitoring locations is basically necessary to effectively ease the real-time processing and interpretation of huge amounts of data arriving at a high sampling rate [29].

2.2.1 Probabilistic-based PMU placement: This paper uses a probabilistic-based method to screen those suitable PMU locations that allows ensuring observability of slow and fast dynamic phenomena in order to accurately perform the vulnerability assessment in real-time. This method was firstly introduced by the authors in [29] and uses MC-based procedures to iteratively evaluate the system fast dynamic coherency and bus oscillatory modal observability, considering the most probable operating scenarios generated from operational statistical information.

The aim of the approach is to determine PMU placement that allows ensuring observability of slow and fast dynamics. Fast coherency clustering allows specifying the candidate buses by means of determining electric coherent areas, and the slow coherency analysis guides the final decision regarding PMU location. Two probabilistic indices are used for this purpose. The measure of orthogonal observability (ORT_{gm}) allows verifying the orthogonality constraint that ensures obtaining as much information as possible about system oscillatory modes; whereas, the average measure of observability (MPO_{gm}) reveals the probabilistic oscillatory observability presented by each bus [29]. Interested readers can find further information regarding the PMU location methodology in [29].

2.2.2 Associated PMU coherent areas: Since fast coherency may change depending on the operating state and the contingency magnitude, the number and the structure of the electric coherent areas might be different. Then, MC-based dynamic simulations and clustering analysis, similar to those applied for placing the PMUs [29], have to be carried out in order to analyse the different possibilities of coherent areas.

In this connection, once PMUs are placed (via the method summarised in 2.2.1), a probabilistic analysis of coherent areas has to be done in order to determine the most representative group of coherent buses associated to each PMU (i.e. the probabilistic areas associated to PMUs), which will permit structuring a database for using in real time (each one of these areas represents the system COIs). This analysis allows determining the most representative group of coherent generators associated to each PMU, whose COI-referred rotor angles will be then computed. Thus, a thorough analysis of the results from MC-based fast dynamic coherency (described in detail in [29]), via histograms, would reveal those generators, belonging to each associated PMU area, that present the highest frequency.

Additionally, since the area arrangement may change depending on the contingency, it is necessary to determine those critical perturbations that cause a significant change in generator coherency. For this purpose, it is suggested to use the same results of the MC-based fast coherency analysis [29] for determining those cases whose results reveal a considerable change in coherency. Hence, a base group of coherency areas (i.e. those of the highest frequency) and several alternative areas depending on the occurrence of one of the critical contingencies are to be specified.

3 Proposed approach for real-time COI-referred rotor-angle estimation and TSI computation

A procedure to estimate COI-referred rotor angles in real time is proposed in this section. It employs SVR to predict the area-based COI-referred rotor angles from selected PMU measurements (i.e. voltage angles and magnitudes). The training tasks are performed using the results obtained from MC-based simulations. These data are subjected to a sampling procedure previous to be used in the SVR training. Additionally, SVR parameter identification is done by using the swarm variant of the mean-variance mapping optimisation ($MVMO^S$).

First, $N-1$ post-contingency dynamic data is generated via MC time domain simulations. MC simulations are performed based on samples from probability distribution functions (PDFs) describing nodal load variations and fault (e.g. three phase short circuits) occurrence rates. The results are then stored throughout the MC repetitions to derive a knowledge database comprising the corresponding COI-referred rotor-angles.

In practice, the database might alternatively be built by using historical records. This database allows offline definition and training of an intelligent COI-referred rotor-angle regressor based on SVR.

For real-time application, the regressor uses post-contingency voltage angles and magnitudes acquired from PMUs to estimate the COI-referred rotor-angles, which allows subsequent computation of the area-based COI-referred rotor angles and a corresponding TSI. Fig. 1 sketches the overall structure of the proposed approach.

3.1 Generation and selection of training data

As stated previously, this paper proposes a MC-based procedure for obtaining the data needed to devise and to train an intelligent regressor, capable of estimating the area COI-referred rotor-angles in real time.

In order to perform MC-based simulations, several input data are required. These data depend on the objective of the simulation, and they are usually represented by their corresponding PDFs. Since the proposal intends to design a wide-area real-time post-contingency situational awareness methodology, capable of being even daily updated by the independent system operator (ISO) in the control centre, the proposed uncertainty analysis encompasses only a specific short-term planning horizon. Thus, the probabilistic models of power system random variables, as well as the grid topology, should be structured within this considered short-term planning horizon, so as to reflect the behaviour of the system as realistic as possible.

In this connection, the basic data to be considered in the MC-based simulation, and which have to be previously prepared by the system operator, are: (i) short-term forecasting of nodal loads; (ii) short-term unit commitment; (iii) short-term system topology; and (iv) occurrence of three phase short circuits in transmission lines, followed by the outage of the faulted line.

The procedure allows considering a significant number of possible operating scenarios, which would ensure robustness of the regressor. In order to obtain realistic data regarding post-contingency dynamic responses, some basic considerations and modelling requirements are taken into account:

- suitable modelling of PDFs (used to randomly generate the input variables considered at every MC repetition): i.e. nodal load demand changes (based on short-term operating scenarios which considers daily load curves), short-term unit commitment of generators, the type of contingency (e.g. short circuit and subsequent line outage), the faulted transmission line and the short circuit location.

doi: 10.1049/iet-gtd.2013.0616

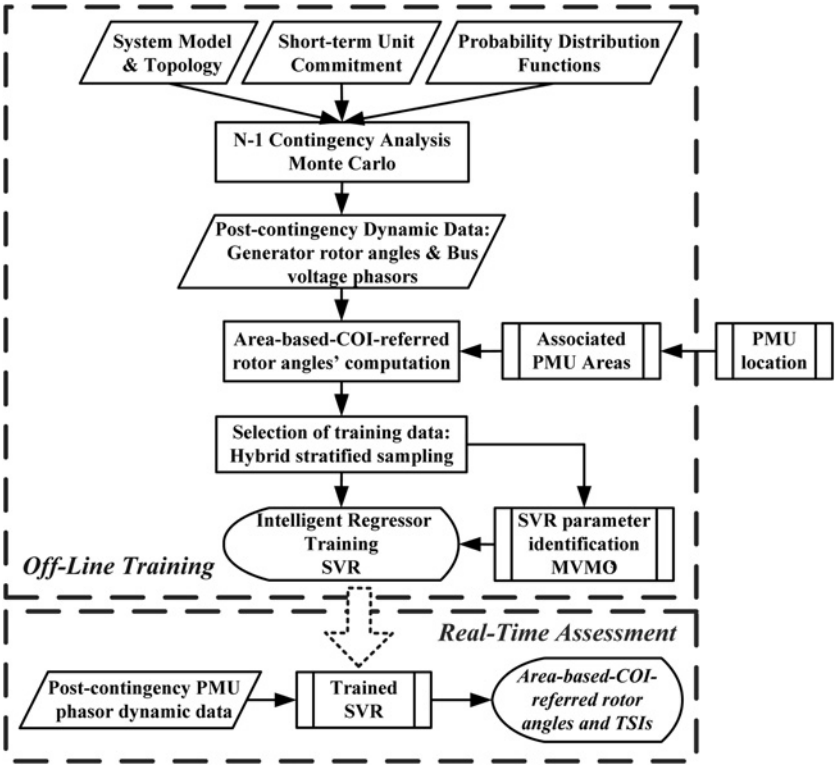

Fig. 1 *Area-based COI-referred-rotor-angle estimation approach*

Three different daily load curves (i.e. typical residential, typical industrial and typical commercial) are employed. These typical load curves are considered to be the results of the corresponding short-term load forecasting performed by the ISO. Fig. 2 illustrates the load curves, for various end-user classes [30], which have been used as nodal loads.

Considering that, regardless of the load forecasting method, the actual system load behaviour will always differ from that obtained from forecasting, the resulted uncertain behaviour of the load has to be considered. Thus, the forecasting uncertainty has been included in the formation of the hourly nodal loads via normal (or Gaussian) distribution functions.

Similarly, the occurrence of three-phase short circuits is assumed to represent independent events, and they are randomly applied at different transmission lines at random locations, followed by the outage of the faulted line. The random faulted element selection and random short-circuit location generation are based on uniform distribution function.

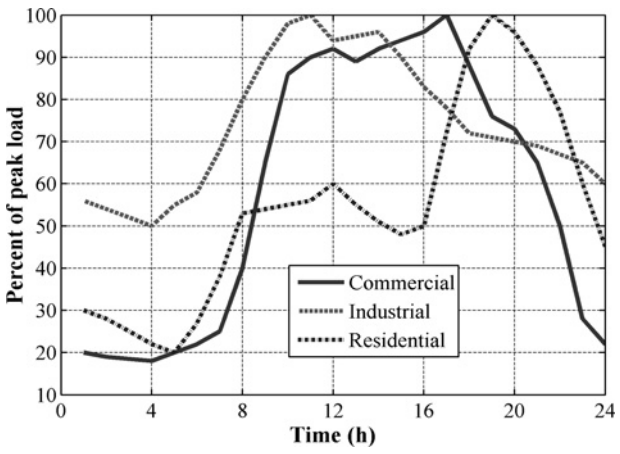

Fig. 2 *Class-specific daily load curves [30]*

- For every trial set of input variables, optimal power flow is carried out in order to define feasible pre-contingency steady-state scenarios. Then, time domain simulations are performed to determine the post-contingency dynamic data to be stored in the knowledge database (which is subsequently used in the regressor training stage).
- Since the simulation time frame depends on the stability phenomenon under study, a 2 s data window is selected in this paper. This window definition is based on the quick evolution of transient instability.
- The accuracy of the regressor directly depends on the suitability of the models to reproduce the phenomenon occurring in the real system. Thus, those components having a significant role in the dynamic system performance (generators, motors, loads, and relevant control systems) have to be modelled with enough detail [31].
- Since the dynamic simulation at every MC repetition will produce a tremendous amount of instantaneous data (due to the several possible scenarios and the fast PMU updating period of few milliseconds), a suitable technique for data sampling has to be used. This paper further proposes a hybrid stratified sampling technique, which is described in the following subsection.

3.1.1 Hybrid stratified sampling method: The huge amount of instantaneous data generated by the MC-based procedure, caused by sampling and evaluation of several possible scenarios as well as the fast PMU updating period of few milliseconds, cannot be jointly used to train the regressor. This issue is of great concern, since the optimisation process involved in the training stage, would

be intractable. A reduction of number of samples is therefore strictly necessary.

In view of this, a hybrid stratified sampling technique, which combines Fuzzy *C*- means (FCM) cluster sampling and the simple random sampling (SRS) algorithms, is proposed in this paper to perform data numerosity reduction. The goal is to obtain a reduced representation of the original data set without losing substantial information [32]. The proposed sampling method is schematically illustrated in Fig. 3.

Fuzzy C-means-based cluster sampling: The aim of cluster sampling is to partition the data into groups or clusters. This technique is more effective for data that can be organised into distinct clusters due to their high diversity, which is the case of this work. When this condition happens, a clustering method (in this case FCM) is applied to the original data to properly select the subsets of data that present similarities [32].

Prior the application of FCM, principal component analysis (PCA) [33] is firstly applied to the data matrix in order to reduce the dimensionality of the data, maintaining as much as possible of the variation presented in them. Next, FCM is applied to the first principal component (PC) scores (which present the desired explained variability [34]) in order to determine the clusters of data representing similar characteristics. Thus, the number of the chosen PCs depends on the desired explained variability degree [34], which is set to be higher than 90% in this paper.

Simple random sampling (SRS): SRS allows a large data set to be represented by a much smaller random sample (or subset) of the data. This paper applies the SRS without replacement (SRSWOR), which is created by extracting s of the N observations of the data set ($s < N$), where the probability of drawing any observation is $1/N$, that is, all observations are equally likely to be sampled [32].

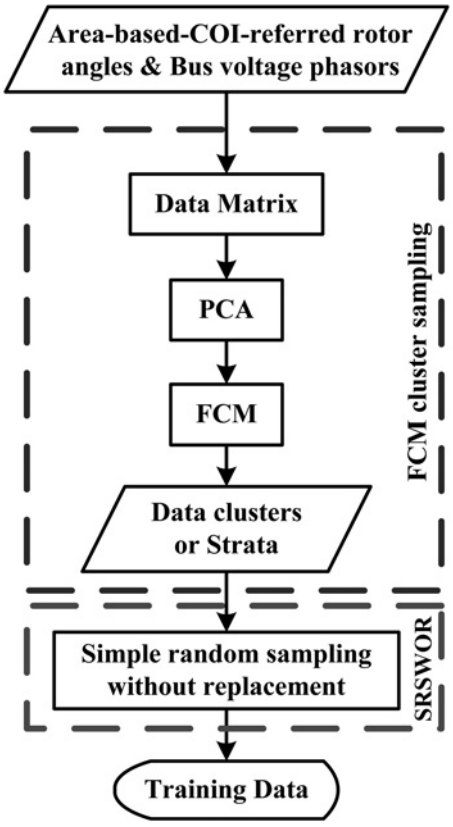

Fig. 3 *Hybrid stratified sampling method*

Hybrid stratified sampling: When data can be divided into mutually disjoint parts (usually called strata), it is possible to generate a stratified sample from them by obtaining a SRS at each stratum. In this way, the method ensures obtaining a representative enough sample, mainly when the data are skewed [32]. In the application given in this paper, the strata constitute the clusters pre-defined by the FCM-based cluster sampling, which are then sampled by SRSWOR.

3.2 Support vector regressor (SVR) training

A function approximation task (regression) consists on determining an input–output relationship using known input–output pairs (x_i, z_i), $i = 1, \ldots, l$, where $x_i \in R^n$ is a feature vector of inputs, $z_i \in R^1$ is the target output, and l is the number of training data [35, 36]. In this case, the input values resemble the MC dynamic data that represent the PMU sampled voltage angles and magnitudes. These data correspond to specific computed COI values, which constitute the regressor output values.

Support vector regression has been chosen to perform this task since it has shown excellent performance in solving function approximation and time series prediction problems [31, 35].

A SVR maps the input space into the multi-dimensional feature space for determining an optimal hyper-plane (OH), which is defined by

$$f(\boldsymbol{x}) = \boldsymbol{w}^{\mathrm{T}} \phi(\boldsymbol{x}) + b \tag{8}$$

where $\boldsymbol{w}$ is the n-dimensional weight vector, $\phi(\boldsymbol{x})$ is the mapping function from $\boldsymbol{x}$ into the feature space, and b is the bias term [35].

In linear regression, the square error function is commonly optimised to achieve the best regression performance. However, poor estimation accuracy could occur when the residuals ($r = z - f(x)$) are relatively large. To overcome this drawback, SVR usually assumes a small positive parameter ε in order to define a piecewise linear function $E(r)$ instead of the square error function [35]

$$E(r) = \begin{cases} 0 & \text{for} \quad |r| \le \varepsilon \\ |r| - \varepsilon & \text{otherwise} \end{cases} \tag{9}$$

Then, the parameter $\varepsilon > 0$ defines the radius of a zone in the input–output space, called the ε-insensitive zone (or tube), and an ideal estimation is achieved when all the training

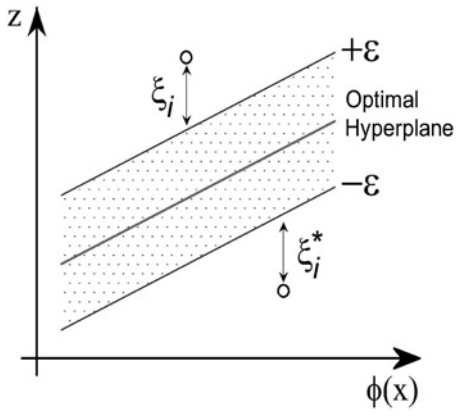

Fig. 4 *SVR OH and its tube*

doi: 10.1049/iet-gtd.2013.0616

data is within this zone. Fig. 4 depicts the ε-insensitive zone, limited by $\pm\varepsilon$, where the non-negative slack variables ξ_i and ξ_i^*, which allow the data outside the tube to exist, are also included.

Mathematically, the support vector regression possesses the following optimisation problem format [36]

$$\begin{aligned} \min_{\boldsymbol{w},b,\xi,\xi^*} \quad & \frac{1}{2}\boldsymbol{w}^{\mathrm{T}}\boldsymbol{w} + C\sum_{i=1}^{l}\xi_i + C\sum_{i=1}^{l}\xi_i^* \\ \text{subject to} \quad & \boldsymbol{w}^{\mathrm{T}}\phi(\boldsymbol{x}_i) + b - z_i \le \varepsilon + \xi_i \\ & z_i - \boldsymbol{w}^{\mathrm{T}}\phi(\boldsymbol{x}_i) - b \le \varepsilon + \xi_i^* \\ & \xi_i,\ \xi_i^* \ge 0, \quad i = 1,\ \ldots,\ l \end{aligned} \tag{10}$$

where $C > 0$ is the margin parameter that determines the trade-off between the distance from the hyper-plane to a data sample (i.e. the margin) and the estimation error.

The mapping function $\phi(\boldsymbol{x})$ is usually defined in terms of the so-called kernel function $K(x_i, x_j)$ (11) [5]

$$K\left(\boldsymbol{x}_i, \boldsymbol{x}_j\right) \equiv \phi\left(\boldsymbol{x}_i\right)^{\mathrm{T}}\phi\left(\boldsymbol{x}_j\right) \tag{11}$$

There are several kernel functions such as linear, polynomial, radial basis function (RBF), among others.

In this paper, RBF kernel is used because this function is capable of handling possible non-linear relations between labels and features [5]. This type of kernel is defined in (12).

$$K\left(\boldsymbol{x}_i, \boldsymbol{x}_j\right) = \mathrm{e}^{-\gamma\|\boldsymbol{x}_i - \boldsymbol{x}_i\|^2}, \quad \gamma > 0 \tag{12}$$

Before training the SVR, it is necessary to identify the best parameters ε and C of (10), and γ of (12). For this purpose, a parameter identification scheme is proposed in this paper based on the swarm variant of the mean-variance mapping optimisation (MVMO^S).

3.2.1 MVMO^S-based SVR parameter identification:

One of the main challenges using SVR is to determine its optimal parameters that entail good accuracy [5]. Traditionally, k-fold cross-validation (CV) procedure and grid-search methodology are used for this purpose [5, 36, 37]. This algorithm iteratively generates a grid of parameters and obtains CV accuracy for each parameter setting [36]. Then, the parameters with the highest CV accuracy are selected. Nevertheless, the grid-search procedure requires a tremendous computational effort. In addition, this approach constitutes a local search method and setting the search interval is a major drawback. Alternatively, best set of parameters can be identified by using a heuristic optimisation algorithm that minimises an appropriately defined objective function (OF). For instance, differential evolution has been applied for this purpose in [38], whereas particle swarm optimisation is used in [39]. The use of heuristic optimisation is motivated by the multi-modal, non-linear and non-convex nature of power system optimisation problems. Along this line, the present paper proposes the application of the swarm variant of the mean-variance mapping optimisation algorithm (MVMO^S) [40] together with 10-fold cross validation to determine the SVR parameters. The SVR parameter identification is sketched in Fig. 5, whereas the optimisation problem is

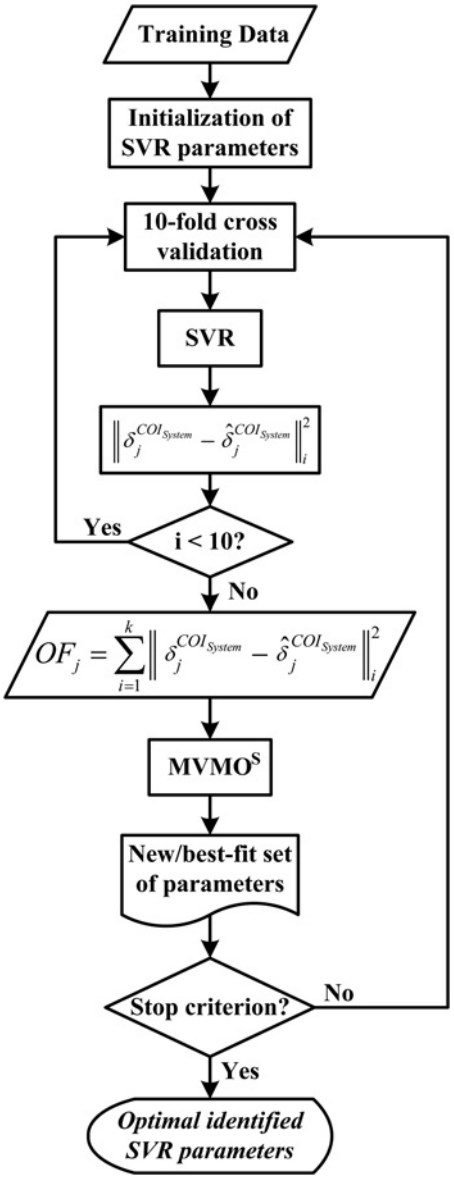

Fig. 5 *MVMO^S-based SVR parameter identification methodology*

summarised by (13) and (14).

Minimize

$$OF_j = \sum_{i=1}^{k}\left\|\delta_j^{\mathrm{COI_{System}}} - \hat{\delta}_j^{\mathrm{COI_{System}}}\right\|_i^2 \tag{13}$$

subjectto:

$$\boldsymbol{x}_{h-\min} \le \boldsymbol{x}_h \le \boldsymbol{x}_{h-\max} \tag{14}$$

where, $\|\cdot\|$ denotes Euclidean norm, whereas $\delta_j^{\mathrm{COI_{System}}}$, $\hat{\delta}_j^{\mathrm{COI_{System}}}$ are the computed COI-referred rotor-angle and the estimated COI-referred rotor-angle of jth area, respectively. The subscript i denotes the ith k-fold ($k = 10$) CV iteration, and $\boldsymbol{x}_h = [\varepsilon,\ C,\ \gamma]$ constitutes the solution to the problem, that is, the set of the optimal SVR parameters. Note that $\mathbf{x}_h$ is part of the intrinsic SVR optimisation process via the solution of (10). Based on the values presented in [38], the search space boundary [$\boldsymbol{x}_{h-\min}$, $\boldsymbol{x}_{h-\max}$] are defined as follows: $C \in [2^{-5}, 2^{15}]$, $\gamma \in [2^{-15}, 2^{5}]$ and $\varepsilon \in [2^{-5}, 2^{0}]$.

3.2.2 SVR training: Once the SVR optimal parameters have been identified, the next step is to train the regressor. For this purpose, the samples determined with the hybrid stratified sampling method and the optimal parameters are used. Afterwards, the regressor is validated using the selected testing data, which simulate the real-time PMU data.

In order to evaluate the performance of the regressor, the mean square error coefficient (MSE) [32] is computed. MSE is the squared norm of the difference between real data and the approximation divided by the number of elements, as shown by (15). The closer this coefficient is to zero, the better the accuracy of the regressor is.

$$\mathrm{MSE} = \frac{\left\| \delta_j^{\mathrm{COI_{System}}} - \hat{\delta}_j^{\mathrm{COI_{System}}} \right\|^2}{N_{\mathrm{samples}}} \tag{15}$$

where, $\|\cdot\|$ denotes Euclidean norm, N_{samples} is the number of testing samples, whereas $\delta_j^{\mathrm{COI_{System}}}$ and $\hat{\delta}_j^{\mathrm{COI_{System}}}$ are the computed COI-referred rotor-angle and the SVR-based estimated COI-referred rotor-angle of the jth area, respectively.

3.3 Real-time implementation and TSI computation

For real-time implementation, the previously offline trained SVR will be in charge of estimating the COI-referred rotor-angles for each area associated to the PMUs, using the actual post-contingency PMU voltage phasors as inputs.

Once the area-COI-referred rotor angles are estimated, and based on the TSA criterion presented in Subsection 2.1, a TSI can be computed in real time. This TSI is set in the range of [0, 1], and is computed for each kth area as shown by (16). This TSI_k will be computed after each set of PMU data arrives to the control center and might be used as an indicator of the imminent area out-of-step.

$$\mathrm{TSI}_k = \begin{cases} 0 & \text{if} \quad \left|\delta_k^{\mathrm{COI_{System}}}\right| < \delta_{\mathrm{lim}} \\ \dfrac{\left|\delta_k^{\mathrm{COI_{System}}}\right| - \delta_{\mathrm{lim}}}{\pi - \delta_{\mathrm{lim}}} & \text{if} \quad \delta_{\mathrm{lim}} \le \left|\delta_k^{\mathrm{COI_{System}}}\right| \le \pi \\ 1 & \text{if} \quad \left|\delta_k^{\mathrm{COI_{System}}}\right| > \pi \end{cases} \tag{16}$$

where TSI_k, and $\delta_k^{\mathrm{COI_{System}}}$ are the TS index and COI-referred rotor-angle in radians of the kth real-time area. Since TSI is conceived to give early warning, it is not necessary to compute it when COI-referred rotor angles are within a normal operating range. Then, the maximum admissible steady-state COI-referred rotor-angle (i.e. the maximum allowed angle determined by steady-state constraints $-\delta_{\mathrm{lim}}$-) is used as the lower limit of the TSI function. This maximum admissible steady-state COI-referred rotor angle, δ_{lim}, is a system parameter that could be easily determined via steady-state simulations such as those described in [41].

Since the final objective of the methodology presented in this subsection is to provide early warning regarding TS problems, the accuracy of the COI-referred rotor angles' estimation becomes more critical when $\mathrm{TSI} > 0$. Therefore, in order to increase the accuracy of the estimation in the range of the critical TSI computation $\left(\text{i.e.} \quad \delta_{\mathrm{lim}} < \left|\delta_j^{\mathrm{COI_{System}}}\right| < \pi\right)$, it is suggested to train and apply a 'verification regressor' when the first regressor estimates that $\left|\delta_j^{\mathrm{COI_{System}}}\right| \in [\delta_{\mathrm{lim}}, \pi]$. This 'verification regressor' has to be also adequately trained. The 'verification regressor' will automatically applied starting from the instant when the first regressor determines that $\left|\delta_j^{\mathrm{COI_{System}}}\right| \in [\delta_{\mathrm{lim}}, \pi]$. Thus, it will replace the first regressor in order to increase the accuracy of the estimation. It is worth mentioning that the training of verification regressor only needs the data set corresponding to the outputs $\left|\delta_j^{\mathrm{COI_{System}}}\right| \in [\delta_{\mathrm{lim}}, \pi]$. The focus on this more specific data set is the reason for obtaining better accuracy results in the range of interest.

Another aspect to be considered is the necessity of training additional regressors due to possible mistakes caused by loss of observability of PMUs as a result of loss of connectivity after specific branch outages. If this type of vagueness occurs, it will be necessary to determine those additional critical branches that provoke the loss of connectivity. For this purpose, TSI has to be computed for each MC scenario, and those scenarios presenting low accuracy results will be then individually analysed. These results can be then compared with the corresponding MC coherency scenario, in order to effectively determine the critical branches that cause the loss of PMU observability.

4 Simulation results

All calculations were performed on a Dell Inspiron personal computer with an Intel® Core™ i3-2350M, 2.30 GHz processing speed, and 6 GB RAM. The proposed approach is tested on the 39 bus New England system [42], slightly modified in order to satisfy the $N-1$ security criterion. First, PMU monitoring locations are selected using the probabilistic method presented in [29]. After performing the complete procedure, it was found out that buses {2, 9, 11, 17, 22, 28} would be the best monitoring locations (interested readers can find a further explanation of these computations in [29]). Fig. 6 shows the single-line diagram of the test system, which highlights the selected PMUs.

Once the PMUs have located, and using the probabilistic fast coherency results (i.e. probabilistic coherent areas), it is possible to determine the most representative areas associated to each PMU and the coherent critical branches, as explained in Subsection 2.2. Fig. 7 presents histograms summarising the frequency of having a given area coherency and showing the generator buses that belong to the same area associated to each selected PMU. In this case, the basic (most common) coherent areas and two additional alternative areas have been specified. The alternative areas depend on the occurrence of two critical contingencies: the outage of line 2–25, and the outage of line 6–11, which causes a significant change in the generator coherency. These results are shown in Table 1.

The aim of determining the basic and alternative COI structures is to adequately select the generators that really keep coherency in each MC iteration in order to obtain a clear database for training the minimum required SVRs, which have been defined as equal to the number of PMUs. Note that there is the possibility of requiring more than six SVRs in this case due to the presence of the alternative COIs when specific outages occur. However, since defining as little as possible regressors will improve the real-time application, only six regressors will be firstly defined and the necessity of extra regressors will be analysed later.

doi: 10.1049/iet-gtd.2013.0616

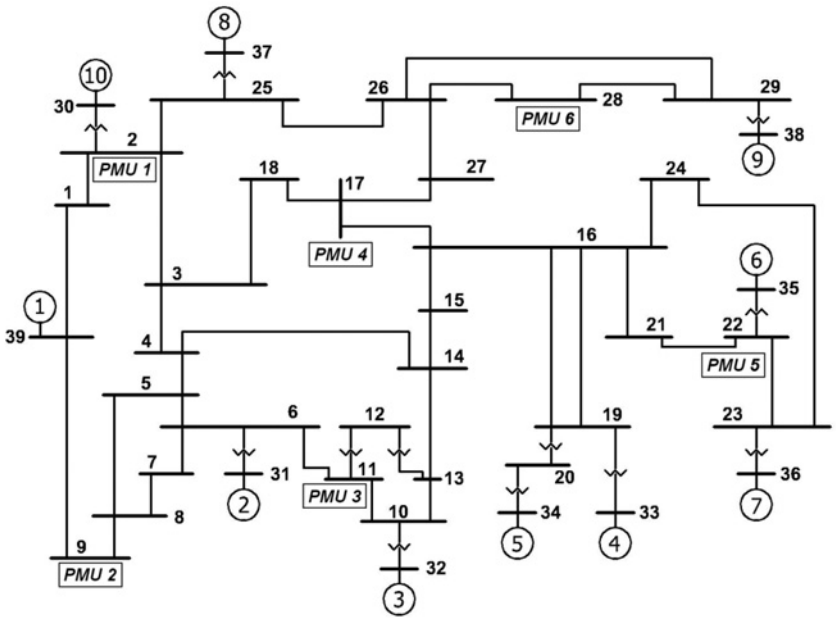

Fig. 6 *39 bus New England test system single-line diagram [42]*

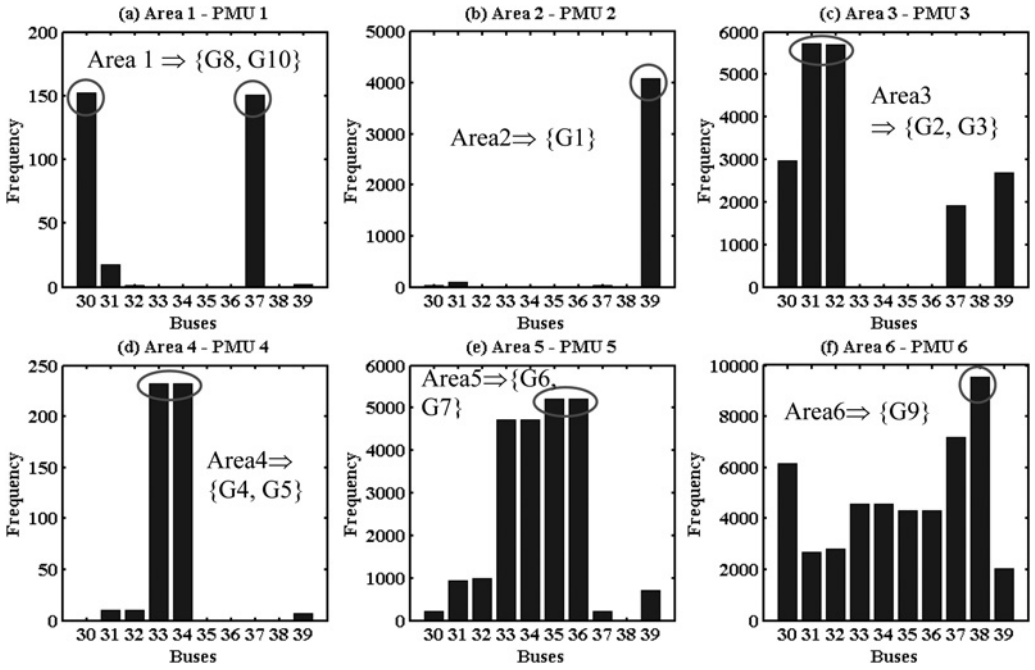

Fig. 7 *Most representative areas associated to each PMU*

Table 1 Most representative associated PMU COIs and critical branches

Coherent area	Generators belonging to associated PMU COIs		
	Basic	Outage L 2–25	Outage L 6–11
area 1	{*G*8, *G* 10}	{*G*10}	{*G*8, *G*10}
area 2	{*G*1}	{*G*1}	{*G*2, *G*1}
area 3	{*G*2, *G*3}	{*G*2, *G*3}	{*G*3}
area 4	{*G*4, *G*5}	{*G*4, *G*5}	{*G*4, *G*5}
area 5	{*G*6, *G*7}	{*G*6, *G*7}	{*G*6, *G*7}
area 6	{*G*9}	{*G*8, *G*9}	{*G*9}

To train the SVR, PMU post-contingency data were firstly generated. For this purpose, dynamic simulations were performed for different scenarios of system loading condition and contingencies sampled from the PDFs of nodal loads and fault occurrence rates. For each scenario, OPF was performed in order to determine the pre-disturbance state, using the functions of the MATPOWER© package [43]. Next, two-second time domain simulations were executed using the routines of DIgSILENT Power Factory© software, considering different disturbances (i.e. three phase short circuits), which were randomly applied at different locations of the transmission lines. The disturbances occurred at 0.12 s, followed by the opening of the corresponding transmission

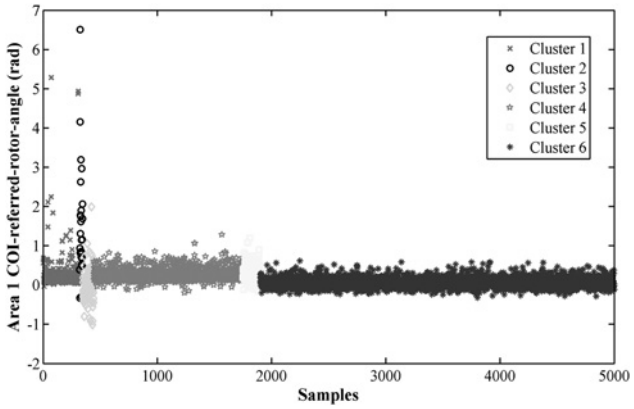

Fig. 8 *Selected COI-referred rotor-angle cluster samples belonging to area 1*

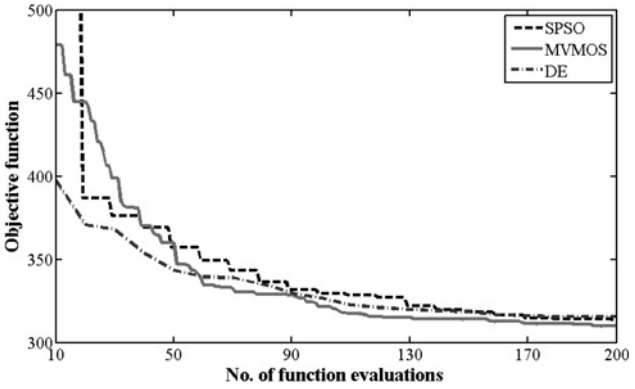

Fig. 9 *Convergence of MVMO^S and other heuristic optimisation methods*

line at 0.2 s. A total of 5000 different scenarios of system loading condition and the contingency occurrence were generated from MC repetitive dynamic simulations. It was assumed that the each PMU has one-cycle updating period (i.e. 16.67 ms). Post-contingency data thus constitutes, at each updating period, the resulting time evolution of rotor angles of all generators, and the voltage phasors (magnitude and angle) of the six buses corresponding to the selected PMU monitoring locations. Besides, using the rotor angles of all generators, and the six representative areas associated to each PMU, the area COI-referred rotor angles were calculated at every MC repetition. These collected area COI-referred rotor angles (outputs) together with the voltage phasors (inputs) constitute the PMU and COI-referred rotor-angle knowledge database, which is used to structure an intelligent COI-referred rotor-angle regressor per area.

For this case study, the PMU and COI-referred rotor-angle database consists of 452 952 observations. Therefore, the proposed hybrid stratified sampling method (Subsection 3.1.1) had to be applied in order to reduce the dimension of the problem to a manageable size level required for training the SVR. Thus, 5000 samples were selected from the complete data set. By using the method, six clusters were defined to which the SRSWOR was subsequently applied. Fig. 8 shows the selected COI-referred rotor-angle samples belonging to Area 1. It is worth to mention that the selection of six clusters allow obtaining well-distributed samples, mainly in the cases where COI-referred rotor angles reach high values, such as those samples belonging to cluster 2 (black circles) in Fig. 8.

The SVR is trained using the reduced set of samples. The target here is to determine the optimal values of the parameters ε and C of (10), and γ of (12) that entail the highest possible accuracy level. Fig. 9 shows the average convergence of the objective function belonging to Area 1 COI-referred rotor-angle, providing additionally comparisons between MVMO^S, differential evolution (DE) [44], and standard particle swarm optimisation (SPSO) [45]. In order to make a fair comparison, each algorithm was independently run for 10 trials with random initialisation of the optimisation variables and static penalty scheme for constraint handling. Note how MVMO^S outperforms all others in terms of both convergence speed and the minimum reached.

Next, the SVR model is trained using the optimal parameters of RBF kernel, and the 5000 samples. Then, it is validated using the testing data (i.e. 100 000 samples selected randomly), which simulate the real-time PMU data. In order to increase the accuracy of the estimation in the range of the critical TSI computation the 'verification regressor' is trained. This regressor is used when the first regressor estimates that $\left|\delta_j^{\mathrm{COI_{System}}}\right| \in [\delta_{\mathrm{lim}}, \pi]$, that is when the estimation turns critical. Then, it is considered that the test power system presents $\delta_{\mathrm{lim}} = \pi/3$.

The performance of the regressor for Area 1 COI-referred rotor-angle during the testing stage is presented in Table 2, which also includes the performance of other regressor algorithms, such as: linear regressor (LR), feedforward neural network regressor (FNNR), and DT regressor (DTR). The performance of the regression is evaluated by computing MSE.

From Table 2, it can be noticed that SVR outperforms all other regressors, which will translate into better regression accuracy. Fig. 10 presents the computed and estimated Area 1 COI-referred rotor-angle time evolution for one unstable case of the MC repetitive dynamic simulations, showing comparisons between SVR, DTR, LR and FNNR. Note the closeness of the estimation (i.e. accuracy) when SVR is applied. Furthermore, it is evidenced that the use of the 'verification regressor' improves the accuracy of all regressors. This is highlighted by the better MSE coefficients in third column of Table 2 as well as by the smoother and more accurate rotor-angle time evolution shown in Fig. 10b.

Additionally, a regression test has been made using only one sample, which would represent a real-time regression at each PMU sample rate. In this instance, the resulting SVR elapsed time is 0.86 ms, which corresponds to the second fastest computation (cf last column of Table 2). The high accuracy and excellent computational speed make SVR superior to all other tested regressors and suitable for real-time applications.

As an illustration, the COI-referred rotor angles for an unstable case are estimated using the final trained

Table 2 Performance of the regression for COI 1

Regressor	MSE single regressor	MSE verification regressor	Elapsed time per regression, ms
DTR	0.017428	0.013637	1.474
LR	0.013393	0.010882	0.121
FNNR	0.008197	0.006854	29.134
SVR	0.006758	0.006160	0.860

doi: 10.1049/iet-gtd.2013.0616

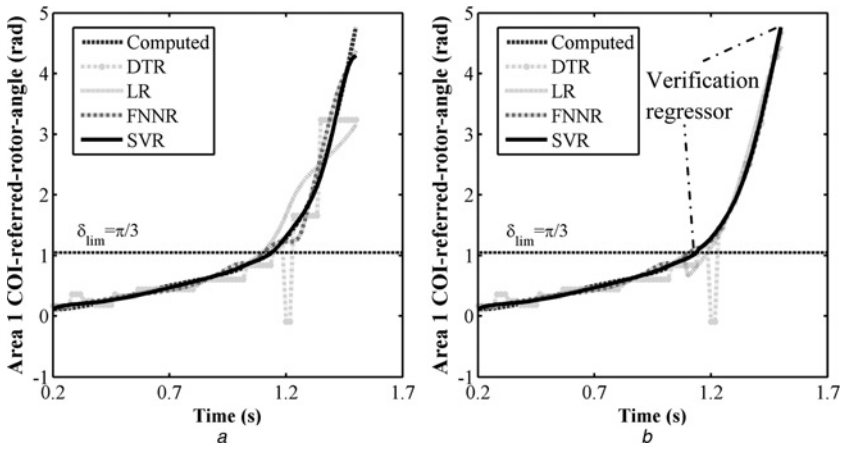

Fig. 10 *Area 1 COI-referred rotor-angle time evolution:*
a Single regressor,
b Verification regressor

regressors. Fig. 11 shows a comparison between the computed (solid lines) and the estimated (dotted lines) associated PMU COI-referred rotor angles for this case. It is possible to appreciate the excellent regression accuracy that agrees with the obtained MSE values.

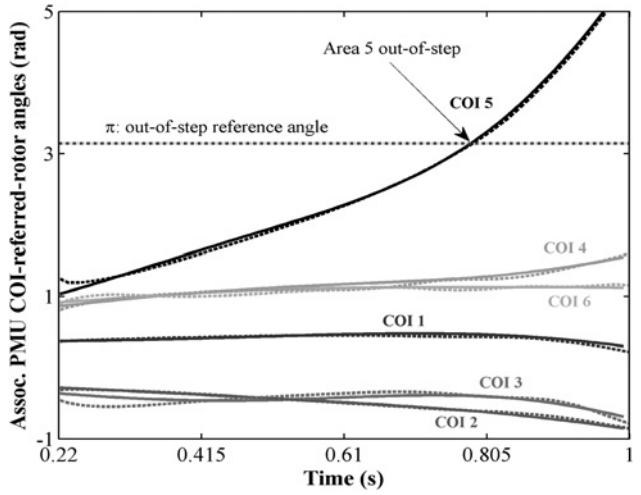

Fig. 11 *Associated PMU COI-referred rotor-angles for a transient unstable case*

After estimation has been carried out, the last step is to calculate the corresponding area-based COI-referred rotor-angle TSIs, which enable ranking the transient instability performance per area. Moreover, these indices might guide the selection of corrective control actions (e.g. fast valving, generation tripping, controlled islanding, etc.) if needed. Table 3 shows a summary of the number of scenarios where TSI reaches a critical value specified as 0.7 in this paper (which has been determined according to MC statistics of out-of-step relay tripping times obtained from simulation), which can be viewed as the corrective control triggering indicator. The concepts of security (i.e. prevent premature or unnecessary control actions) and dependability (i.e. perform corrective control when needed) are used for analysing the performance of the TSI estimation.

Results from Table 3 highlight the excellent performance and effectiveness of the proposed approach regarding security, since it would allow precluding unnecessary control actions. On the other hand, it implies dependability greater than 90%, which is desirable for wide-area control strategy.

Although the percentage of dependability is good enough for wide-area applications, an analysis of the misdetections will allow determining the weakness of the approach as well as suggesting possible improvements. Namely, there were 88 cases leading to wrong control actions. A thorough analysis revealed that 77 of these cases correspond to the

Table 3 TSI estimation performance

$0 \le TSI < 0.7$		$0.7 \le TSI \le 1$		Security, %	Dependability, %
Simulated	Estimated	Simulated	Estimated		
4056	4144	944	856	100	90.68

Table 4 TSI estimation performance including area 5 and area 6 specific regressors

$0 \le TSI < 0.7$		$0.7 \le TSI \le 1$		Security, %	Dependability, %
Simulated	Estimated	Simulated	Estimated		
4056	4060	944	940	100	99.58

fault and opening of line 22–23, with a consequent loss of synchronism of *G*7. This instability cannot be monitored from PMU 5 due to the loss of grid connectivity. Similarly, other 7 cases correspond to the fault and opening of line 28–29 resulting in the loss of synchronism of *G*9, which causes the loss of observability from PMU 6. These results agree with the need of determining the critical branches that have been treated in Subsection 2.2.

From the analysis, the approach has slight drawbacks when the areas possess a poorly meshed grid that could involve adverse implications regarding feeble PMU measurement observability due to loss of connectivity. In order to overcome this problem, it is recommended to train an additional specific regressor only for those cases in which areas present poorly meshed characteristics caused by opening of specific branches (i.e. critical branches). For the system under study, two specific regressors were additionally trained: (i) for area 5, when line 22–23 is triggered and (ii) for area 6, when line 28–29 is opened. Table 4 presents a summary of the number of cases where the TSI reaches critical values, considering the inclusion of both specific regressors. It is possible to appreciate how dependability increases to more than 99%, highlighting the good performance of the proposed improvement to account for cases in which an area has poorly meshed characteristics.

It is important to highlight in this part that, as noticed at the beginning of this subsection, some branch outages can affect the accuracy of the regression due to the considerable change of coherency or loss of connectivity. For this system, a total of eight different regressors (and their corresponding verification regressors), have been trained. From these regressors, six correspond to the associated PMU COIs and two derive from the loss of connectivity caused by the outage of two branches (i.e. line 22–23 and line 28–29). For this power system, it did not necessary to train additional regressors for the change of coherency caused by the outage of line 2–25 and line 6–11.

5 Discussion

In order to highlight the approach presented in this paper, a fair comparison is performed with the E-SIME method [16]. For this purpose, a case study corresponding to the fault and opening of line 28–29, which results in the loss of synchronism of *G*9, described in the previous section, is simulated by applying the E-SIME method.

Thus, simulations consist on the prediction of transient instability after the occurrence of a three phase short circuit at 0.12 s in line 28–29 near bus 29. The prediction calculations start once the fault is cleared at 0.2 s and consider at least three measurements at the time point $tk - 2\Delta t$, $tk - \Delta t$ and tk.

First, the critical machines are determined by means of the data mining-based approach presented in [16]. After identifying the critical machines (in this case *G*9) [16], the next step aims at determining the parameters of the OMIB, that is, the accelerating power P_a and rotor-angle δ at the instants $tk - 2\Delta t$, $tk - \Delta t$ and tk. This task is repeated if the new data of a subsequent point of time is added to the already collected information. The resulting estimated $P_a - \delta$ curves are illustrated in Fig. 12. These curves present better approximations with respect to the real curve (red dotted continuous line) when more measurement points are considered by the prediction algorithm.

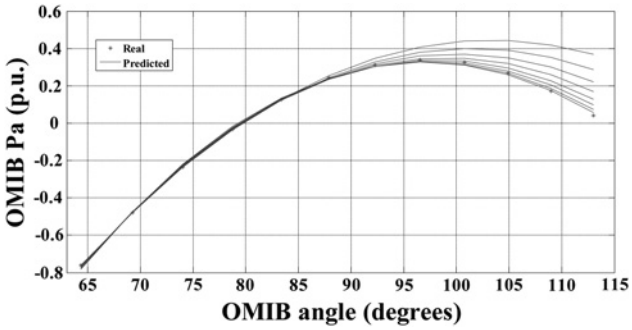

Fig. 12 *Prediction of the Pa-δ curve of the OMIB equivalent*

Table 5 Prediction and assessment of TS via E-SIME

t_k, s	η	t_u, s
0.300	>0	—
0.320	−1.302	0.435
0.340	−3.531	0.430
0.360	−5.398	0.427
0.380	−6.877	0.426
0.400	−7.913	0.426
0.420	−8.433	0.426

Table 5 lists values for different subsequent instants *tk* (points of time at which a measurement is received) as well as the corresponding estimated unstable margin η and time to instability t_u. The results listed in the table were obtained after detecting an unstable condition, which occurs after 300 ms in this particular case. Note that the time t_u, in which the instability is predicted (i.e. first negative value of η), is considerably short (around 435 ms). Thus, for $tk =$ 300 ms, there would be approximately 135 ms remaining to perform a control action, which suggest the implementation of a scheme at the control centre for execution of countermeasures in an automatic manner.

From the previous results, E-SIME effectively provides adequate early warning as regards TS risk, allowing also the identification of the critical machine. Comparing these results with those obtained by applying the method proposed in this paper, both methodologies are capable of giving early warning to the system, identifying the generator that is going out of step (E-SIME), or the electric area that is losing synchronism (COI-referred rotor angles), respectively.

Although the results could be considered as equivalent, it is worth mentioning that while most of the information required by E-SIME is supposed to be provided by PMUs, these devices do not deliver information directly usable by E-SIME. That is not only because they are connected to the high voltage buses, instead of the machines' buses, but also because they measure electrical variables (voltages and currents), while the quantities needed are machines' rotor angles (mechanical variables) and electrical powers [17]. On the other hand, the proposed approach allows estimating the COI-referred rotor angles from PMUs adequately located throughout the system, which constitutes a great improvement as regards the E-SIME limitation.

6 Conclusions

Real-time TSA is a fundamental task within the framework of a self-healing grid structure. Accordingly, this paper proposes

doi: 10.1049/iet-gtd.2013.0616

a novel approach for post-contingency area-based centre-of-inertia (COI) referred rotor angles estimation from PMU measurements. To this aim, several offline tasks were addressed to deal with issues regarding the selection of PMU monitoring locations, reduction of data numerosity, as well as definition, training and tuning of a suitable regressor.

The first task is accomplished by using a MC-based procedure that accounts for uncertainties of nodal load variations and fault occurrence rates to determine those PMU locations providing the highest observability. Besides, a hybrid stratified sampling technique, which couples FCM cluster sampling and the SRS algorithms, is proposed to tackle data numerosity reduction. The MC framework was also used for repetitive evaluation of power system TS performance in order to structure a knowledge database (comprising PMU data and COI-referred rotor-angle), which serves to devise an intelligent COI-referred rotor-angle regressor per system area. A SVR regressor is adopted to predict area-based COI-referred rotor angles from PMU measurements acquired in real time.

The regressor is tuned using the swarm mean-variance mapping optimisation, a heuristic algorithm exhibiting fast convergence and enhanced exploration features. Performance comparisons with other regressors, based on numerical tests on the IEEE New England 39-bus system, demonstrate that SVR provides high accuracy and excellent computational speed, which are highly desirable for the targeted real-time estimation. Furthermore, the use of the regressor would involve a high confidence level to assist control decision making depending on real-time post-disturbance evolution of power system TS performance. The implementation of the approach in a real large-size interconnected power system is being currently pursued.

7 References

1 Andersson, G., Donalek, P., Kamwa, I., Kundur, P., *et al.*: 'Causes of the 2003 major grid blackouts in North America and Europe, and recommended means to improve system dynamic performance', *IEEE Trans. Power Syst.*, 2005, **20**, (4), pp. 1922–1928

2 Amin, M.: 'Toward self-healing infrastructure systems' (Electric Power Research Institute (EPRI), IEEE, 2000)

3 Kundur, P., Paserba, J., Ajjarapu, V., *et al.*: 'Definition and classification of power system stability IEEE/CIGRE joint task force on stability terms and definitions', *IEEE Trans. Power Syst.*, 2004, **19**, (3), pp. 1387–1401

4 Echeverria, D., Rueda, J., Colomé, G., Erlich, I.: 'Improved method for real-time transient stability assessment of power systems'. Proc. IEEE PES General Meeting, San Diego, California, July 2012

5 Cepeda, J., Colomé, G., Castrillón, N.: 'Dynamic vulnerability assessment due to transient instability based on data mining analysis for smart grid applications'. Proc. IEEE PES ISGT-LA Conf., Medellín, Colombia, October 2011

6 Savulescu, S., Virmani, S., Arnold, L., *et al.*: 'Real-time stability assessment in modern power system control centers' (IEEE Press Series on Power Engineering, 2009)

7 Huang, Z., Zhang, P., Baldick, R., *et al.*: 'Vulnerability assessment for cascading failures in electric power systems'. Task Force on Cascading Failures, Proc. IEEE PES Power Systems Conf. and Exposition, Seattle, 2009

8 Liu, C.W., Thorp, J.: 'Application of synchronised phasor measurements to real-time transient stability prediction', *IEE Proc. Gener. Transm. Distrib.*, 1995, **142**, (4), pp. 355–360

9 Liu, C.W., Thorp, J.S.: 'New methods for computing power system dynamic response for real-time transient stability prediction', *IEEE Trans. Circuits Syst. I, Fundam. Theory Appl.*, 2000, **47**, (3), pp. 324–337

10 Liu, C.W., Su, M.C., Tsay, S.S., Wang, Y.J.: 'Application of a novel fuzzy neural network to real-time transient stability swings prediction based on synchronized phasor measurements', *IEEE Trans. Power Syst.*, 1999, **14**, (2), pp. 685–692

11 Yamashita, K., Kameda, H.: 'Out-of-step prediction logic for wide-area protection based on an autoregressive model'. Proc. 2004 IEEE PES Power Systems Conf. & Exposition, vol. 1, New York, USA, pp. 307–312

12 Soman, S.A., Nguyen, T.B., Pai, M.A., Vaidyanathan, R.: 'Analysis of angle stability problems: a transmission protection system perspective', *IEEE Trans. Power Deliv.*, 2004, **19**, (3), pp. 1024–1033

13 Liu, M., Sun, H., Zhang, B., Yao, L.: 'PMU measurements and EMS models based transient stability on-line forecasting'. Power & Energy Society General Meeting, PES '09, 2009

14 Wang, Y., Yu, J.: 'Real time transient stability prediction of multi-machine system based on wide area measurement'. Power and Energy Engineering Conf., APPEEC 2009, Asia-Pacific, 2009

15 Echeverría, D., Colomé, G.: 'Evaluación en tiempo real de la Estabilidad Transitoria de SEP utilizando mediciones sincrofasoriales'. Proc. XIV ERIAC, Ciudad del Este, Paraguay, June 2011

16 Echeverría D., Rueda J., Cepeda J., Colomé D., Erlich I.: 'Comprehensive approach for prediction and assessment of power system transient stability in real-time'. IEEE PES ISGT Europe, Denmark, October 6–9, 2013

17 Glavic, M., Ernst, D., Ruiz-Vega, D., Wehenkel, L., Pavella, M.: 'E-SIME- a method for transient stability closed-loop emergency control: achievements and prospects'. Proc. of the IREP Symp. 2007, Bulk Power System Dynamics and Control VII –'Revitalizing Operational Reliability', 19–24 August 2007, Charleston South Carolina, USA

18 Makarov, Y., Miller, C., Nguen, T., Ma, J.: 'Characteristic ellipsoid method for monitoring power system dynamic behavior using phasor measurements'. Proc. VII Symp. on Bulk Power System Dynamics and Control, Charleston, USA, August 2007

19 Gomez F.: 'Prediction and control of transient instability using wide area phasor measurements'. PhD thesis, University of Manitoba, September 2011

20 Kamwa, I., Beland, J., Mcnabb, D.: 'PMU-based vulnerability assessment using wide-area severity indices and tracking modal analysis'. IEEE Power Systems Conf. and Exposition, 139-149, Atlanta, November 2006

21 Kamwa, I., Grondin, R., Loud, L.: 'Time-varying contingency screening for dynamic security assessment using intelligent-systems techniques', *IEEE Trans. Power Syst.*, 2001, **16**, (3), pp. 526–536

22 Kamwa, I., Pradham, A.K., Joos, G.: 'Automatic segmentation of large power systems into fuzzy coherent areas for dynamic vulnerability assessment', *IEEE Trans. Power Syst.*, 2007, **22**, (4), pp. 1974–1985

23 Kamwa, I., Pradham, A.K., Joos, G., Samantaray, S.R.: 'Fuzzy partitioning of a real power system for dynamic vulnerability assessment', *IEEE Trans. Power Syst.*, 2009, **24**, (3), pp. 1356–1365

24 Kamwa, I., Samantaray, S.R., Joos, G.: 'Development of rule-based classifiers for rapid stability assessment of wide-area post-disturbance records', *IEEE Trans. Power Syst.*, 2009, **24**, (1), pp. 258–270

25 Kamwa, I., Samantaray, S.R., Joos, G.: 'Catastrophe predictors from ensemble decision-tree learning of wide-area severity indices', *IEEE Trans. Smart Grid*, 2010, **1**, (2), pp. 144–158

26 Kamwa, I., Samantaray, S.R., Joos, G.: 'On the accuracy versus transparency trade-off of data-mining models for fast-response PMU-based catastrophe predictors', *IEEE Trans. Smart Grid*, 2012, **3**, (1), pp. 152–161

27 Kundur, P.: 'Power system stability and control' (McGraw-Hill, New York, USA, 1994)

28 Izzri, N., Wahab, A., Mohamed, A.: 'Area-based COI-referred rotor angle index for transient stability assessment and control of power systems'. Hindawi Publishing Corporation, Abstract and Applied Analysis, Volume 2012, available at: http://www.hindawi.com/journals/aaa/2012/410461/

29 Cepeda, J., Rueda, J., Erlich, I., Colomé, G.: 'Probabilistic approach-based PMU Placement for real-time power system vulnerability assessment'. Proc. ISGT PES Europe, Berlin, October 2012

30 Iowa State University: 'Loads and load duration'. academic notes. Available at: http://www.ee.iastate.edu/~jdm/ee455/notes2_loads.doc

31 Dong, Z., Zhang, P.: 'Emerging techniques in power system analysis' (Springer, 2010)

32 Han, J., Kamber, M.: 'Data mining: concepts and techniques' (Elsevier, Morgan Kaufmann Publishers, 2006, 2nd edn.)

33 Jollife, I.: 'Principal component analysis' (Springer, 2002, 2nd edn.)

34 Rueda, J., Cepeda, J., Erlich, I.: 'Estimation of location and coordinated tuning of PSS based on mean-variance mapping optimization'. IEEE PES General Meeting, San Diego, California, July 2012

35 Abe, S.: 'Support vector machines for pattern classification' (Springer, 2010, 2nd edn.)

36 Chang, C.-C., Lin, C.-J.: 'LIBSVM: a library for support vector machines'. 2001. Software available at: http://www.csie.ntu.edu.tw/~cjlin/libsvm

37 Ye, S., Zheng, Y., Qian, Q.: 'Transient stability assessment of power system based on support vector machine'. Atlantis Press, available at: http://www.atlantis-press.com/php/download_paper.php?id=1340

38 Kalyani, S., Swarup, K.: 'Classification and assessment of power system security using multiclass SVM', *IEEE Trans. Syst. Man and Cybernetics, C: Appl. Rev.*, 2011, **41**, (5), pp. 753–758

39 Cepeda, J., Ramirez, D., Colome, G.: 'Probabilistic-based overload estimation for real-time smart grid vulnerability assessment'. Proc. Sixth IEEE/PES Transmission and Distribution: Latin America Conference and Exposition (T&D-LA), 2012, Montevideo, Uruguay, September 2012

40 Erlich, I.: 'Mean-variance mapping optimization algorithm home page'. Software available at: http://www.uni-due.de/mvmo/

41 Cepeda, J., Verdugo, P.: 'Determinación de los Límites de Estabilidad Estática de Ángulo del Sistema Nacional Interconectado'. *Revista Técnica Energía*, 2014, **10**, (1), pp. 5–12

42 Pai, M.: 'Energy function analysis for power system stability' (Kluwer Academic Publishers, 1989)

43 Zimmerman, D.: 'MATPOWER'. PSERC. Software available at: http://www.pserc.cornell.edu/matpower

44 Buehren, M.: 'Differential evolution'. Software available at: http://www.mathworks.com/matlabcentral/fileexchange/18593-differential-evolution%20

45 Omran, M.: 'SPSO 2011'. Software available at: http://www.particleswarm.info/Programs.html#SPSO_2011_Matlab

doi: 10.1049/iet-gtd.2013.0616